shows a comparison of results for $\theta = 0°$, with $T_s = 400$ and 100 K. These observations suggest that for the higher surface temperature, the HCl product is formed through two distinct reaction mechanisms, one of which is "frozen out" at the lower surface temperature.

We obtained further dynamical evidence for these two assumed mechanisms by changing the energy of the incident H beam and from the form of the angular distributions. For $\theta = 0°$, changing the mean energy of the incident H atoms from 0.07 to 0.3 eV results in an increase in the mean translational energy of the HCl product from ~0.50 to ~0.56 eV. Such behavior clearly indicates an essentially direct reaction process. The angular distributions support this model. The angular distributions of the fast component for H atom beams with mean energies of 0.07 and 0.3 eV are shown in Fig. 5. The fact that these distributions are asymmetric with respect to the surface normal and that they change with the incidence energy implies that the HCl product retains a memory of the momentum of the incident H atom. Such a result is inconsistent with an LH mechanism but rather shows that the reaction occurs directly, by way of an ER mechanism. We obtained further information by analyzing TOF distributions obtained at different values of $\theta$ for the 0.3-eV beam. We find that the mean energy of the HCl product associated with the fast component rises to ~0.8 eV for values of $\theta$ of ~20° on either side of the normal. This behavior indicates that there is a strong correlation between the exit angle and the energy released in translation. A study of such effects as a function of incidence energy might elucidate this behavior.

In contrast to the fast component, the angular distribution of the slow component is found to be symmetric with respect to the surface normal, following a distribution that is slightly narrower than a cosine. The actual distribution is well described by a cosine function raised to the power of 1.4. The slight narrowing with respect to a true cosine is somewhat surprising. One possibility is that this component contains a small contribution from an ER-type mechanism that involves multiple "bounces" (*17*). Ideally, such questions could be better addressed by measuring angle and velocity distributions for products in specific quantum states.

Many questions remain for this system: Does the ER channel involve a single collision or can the H atom "bounce" before reacting? Why do some collisions lead to ER and others to LH mechanisms? What determines the branching ratio? Our results, together with other recent studies (*7–11*), set a firm foundation for such questions. We believe that such dynamical studies are a prerequisite to understanding surface chemistry in terms of atomic and molecular motions.

## REFERENCES

1. See, for example, W. H. Weinberg, in *Dynamics of Gas-Surface Interactions*, C. T. Rettner and M. N. R. Ashfold, Eds. (Royal Society of Chemistry, London, 1991), pp. 171–219.
2. I. Langmuir, *Trans. Faraday Soc.* **17**, 621 (1922).
3. C. C. Cheng, S. R. Lucas, H. Gutleben, W. J. Choyke, Y. T. Yates, *J. Am. Chem. Soc.* **114**, 1249 (1992).
4. M. Xi and B. E. Bent, *J. Vac. Sci. Technol. B* **10**, 2440 (1992).
5. P. Kratzer and W. Brenig, *Surf. Sci.* **254**, 275 (1991).
6. B. Jackson and M. Persson, *J. Chem. Phys.* **96**, 2378 (1992).
7. C. T. Rettner, *Phys. Rev. Lett.* **69**, 383 (1992).
8. E. W. Kuipers, A. Vardi, A. Danon, A. Amirav, *ibid.* **66**, 116 (1991).
9. R. I. Hall, I. Cadez, M. Landau, F. Pichou, C. Schermann, *ibid.* **60**, 337 (1988).
10. P. J. Eenshustra, J. H. M. Bonnie, J. Loss, H. J. Hopmann, *ibid.*, p. 341.
11. K. Lykke and B. D. Kay, in *SPIE Proc.* **1208**, 18 (1990).
12. C. T. Rettner, L. A. DeLouise, D. J. Auerbach, *J. Chem. Phys.* **85**, 1131 (1986).
13. G. N. Kastanas and B. E. Koel, *Appl. Surf. Sci.* **64**, 235 (1993).
14. C. T. Rettner, H. A. Michelsen, D. J. Auerbach, C. B. Mullins, *J. Chem. Phys.* **94**, 7499 (1991).
15. D. J. Auerbach and C. T. Rettner, *Rev. Sci. Instrum.* **63**, 3939 (1992).
16. C. T. Rettner, E. K. Schweizer, C. B. Mullins, *J. Chem. Phys.* **90**, 3800 (1989).
17. J. Harris and B. Kasemo, *Surf. Sci.* **105**, L281 (1981).

27 September 1993; accepted 17 November 1993

---

# High-Performance Photorefractive Polymers

Martin Liphardt, Arosha Goonesekera, Brian E. Jones,
Stephen Ducharme,* James M. Takacs, Lei Zhang

**Photorefractive materials can form "instant" holograms without time-consuming development steps. Their potential applications include image processing, optical data storage, and correction of image distortion, but the cost of crystal growth and preparation has been a primary impediment to commercial application. Polymers, on the other hand, are low in cost and readily fabricated in a variety of forms. Photorefractive polymers were constructed with performance that matched or exceeded the performance of available photorefractive crystals. The largest observed two-beam energy coupling gain coefficient for the polymers was 56 per centimeter.**

The photorefractive effect, a persistent but reversible change in the refractive index of an electrooptic material caused by nonuniform illumination, was first observed as a detrimental "optical damage" in lithium niobate and other crystals used for second harmonic generation (*1*). The photorefractive effect occurs in materials that have the following three properties: (i) photoconduction, (ii) photosensitive traps, and (iii) linear electrooptic response. Nonuniform illumination liberates charges from the photosensitive traps in the bright regions. These charges diffuse and drift until they recombine with ionized traps elsewhere. After some time, charge is depleted from the bright regions and added to the dark regions, creating a spatially varying, or space-charge, electric field. The space-charge electric field changes the index of refraction through the linear electrooptic (Pockels) effect, creating a replica, or phase hologram, of the original intensity pattern. This hologram persists in the dark. Photorefractive materials can be used in image processing applications such as image correlation (*2*), amplification (*3*), and dynamic novelty filtering (*4*). Data can be stored in photorefractive materials in the form of the three-dimensional phase holograms, which have very high density and can be accessed by fast parallel optical retrieval (*5*) or associative retrieval with incomplete addressing (*6*). Photorefractive materials have been used to correct phase distortions suffered by an optical beam in inhomogeneous (*7*) or turbulent media (*8*). These and many other applications have been demonstrated with high-performance photorefractive crystals.

Polymers that exhibit the photorefractive effect have been made (*9–12*). These hybrid materials combine electrooptic polymers with charge transport agents and photosensitizing dyes. Photorefractive polymers may replace crystals in future applications because of their relative low cost. Polymers are also amenable to mass production in a variety of forms satisfying complex requirements imposed by device performance and operating environment; polymers can be cast, spun, painted, molded, injected, or extrud-

---

M. Liphardt, A. Goonesekera, B. E. Jones, S. Ducharme, Department of Physics and Astronomy, University of Nebraska, Lincoln, NE 68588–0111.
J. M. Takacs and L. Zhang, Department of Chemistry, Center for Materials Research and Analysis, University of Nebraska, Lincoln, NE 68588–0304.

*To whom correspondence should be addressed.

ed, and they can be patterned by common lithographic techniques. It is necessary, however, to further improve the performance of photorefractive polymer mixtures beyond these first demonstrations to compete with the performance of available crystals (*13*).

This report describes a photorefractive polymer with performance competitive with available crystals. The polymer has a large two-beam energy coupling gain coefficient, an important measure of photorefractive performance. This high performance has been realized because we could apply higher electric fields than in previous studies to thick (>100 μm) samples. The same polymer was previously shown to have increased speed of operation (*14, 15*), another important measure of photorefractive performance. The measured gain coefficients are much larger than in the first reported photorefractive polymer (9) and five times as large as the gain coefficients reported in another photorefractive polymer (*16*).

The polymer is a mixture of the electrooptic polymer bisphenol A 4,4′-nitroaminostilbene (BisA-NAS) (*11*) with 29% by weight benzaldehyde diphenyl-hydrazone (DEH), a hole transport agent (*17*). The BisA-NAS polymer and the hole transport agent DEH are shown in Fig. 1. The BisA polymer backbone acts as the physical binder but is otherwise optically and electrically inert. The stilbene dye substituent NAS plays two roles in these polymers: As a source of charges and, when aligned in a static electric field, the NAS molecules produce the necessary bulk linear electrooptic response. The DEH transport agent transfers the charge generated at the dye molecules to other parts of the material, thus completing the process of photoconduction. The samples consist of 145-μm-thick polymer films formed between two glass plates that are coated with transparent indium-tin-oxide electrodes and thin polyvinyl alcohol electrical buffer layers (samples without buffer layers had comparable performance). Sample fabrication is described in more detail elsewhere (*9, 11, 15*). The increased applied static electric field in the polymer is responsible for the 100-fold increase of the gain coefficient from 0.5 cm$^{-1}$ to 56 cm$^{-1}$.

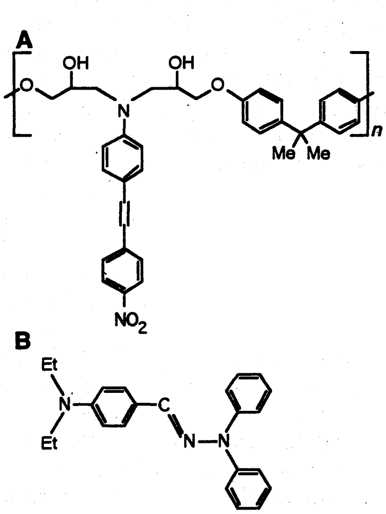

**Fig. 1.** (**A**) The electrooptic polymer BisA-NAS, and (**B**) the hole transport agent DEH. Me, methyl; Et, ethyl.

In two-beam energy coupling, the transmitted intensity of the probe beam 2 is monitored while a second, mutually coherent, pump beam 1 intersects it in the photorefractive material (Fig. 2). The intensity of the probe beam as it exits the sample is given by the expression (*18*)

$$I = I_o \frac{(1 + \beta)e^{gL'}}{1 + \beta e^{gL'}} \tag{1}$$

where *I* is the exit intensity of the weak probe beam 2 in the presence of the strong pump beam 1 with exit intensity $I_p$ and $I_o$ is the exit intensity in its absence. The beam ratio $\beta = I_o/I_p$, *g* is the two-beam energy coupling gain coefficient, and $L' = 160$ μm is the effective path length of the beams in the sample. [The tilted geometry was necessary to achieve proper electrooptic response which requires a nonzero projection of the grating wave vector along the applied static electric field (9).] The illumination, with 1.0-mm beam diameter and total intensity ~1 W/cm$^2$, was generated by a TEM$_{00}$ continuous wave dye-laser. The grating spacing was $\Lambda = 2.6$ μm, the grating wave vector **k** ($|\mathbf{k}| = 2\pi/\Lambda$) was oriented 63.6° from the sample normal, and the effective path length of the beams in the sample was 160 μm at a wavelength of 650 nm (*19*). At the largest observed gain coefficient of 56 cm$^{-1}$, the transmitted intensity of the probe beam increased more than twofold, $I/I_o = 2.2$. We verified that the observed gratings were photorefractive phase gratings, and not absorption gratings, by measuring the exchange of power (or energy) between the beams with about equal intensities ($\beta \approx 1$). In all cases one beam lost power and the other beam gained an equal amount of power so that the total power was constant. Furthermore, we rapidly translated the sample [a method described in (*10*)] and observed the same asymmetric behavior. This means that energy is transferred from one beam to the other in contrast with the case of an absorption grating where both beams experience gain (or loss) simultaneously. The measurements described below were made with the probe beam 2 much weaker than the pump beam 1 ($\beta << 1$) because the space-charge distribution of large modulation ($\beta \approx 1$) gratings is nonsinusoidal, and the amplitude of the fundamental grating component is consequently depleted (*18*).

The two-beam energy coupling gain coefficient *g* of a sample of BisA-NAS:DEH 29% is shown for $\beta = 0.114$ (Fig. 2) and applied static electric fields ranging from −655 kV/cm to +620 kV/cm. The solid line in Fig. 2 is a fit to the data according to a theoretical expression derived in the following way. The gain coefficient (*18*) is proportional to the space-charge electric field $E_{sc}$ and to the electrooptic coefficient $r_{eff}$, which in turn is proportional to the applied static electric field $E_a$ (9). The gain coefficient is

$$g = \frac{\pi n_o^3}{\lambda \cos\theta'} r_{eff} \frac{1}{m} E_{sc} \tag{2}$$

and the space-charge electric field $E_{sc}$ is given by (*20*)

$$E_{sc} = mE_q \sqrt{\frac{E_o^2 + E_d^2}{E_o^2 + (E_d + E_q)^2}} \tag{3}$$

where $n_o$ is the average index of refraction (*19*), $\lambda = 650$ nm is the vacuum wavelength, $2\theta'$ is the angle between the two beams inside the sample, $m = \sqrt{\beta}\cos(\theta')/(1 + \beta)$ is the modulation depth, $E_o = E_a \cos(63.6°)$ is the component of the applied static electric field along the grating wave vector **k**, $E_q = eN_{PR}/(\epsilon_r\epsilon_o k)$ is the limiting space-charge electric field (the value of $E_{sc}$ achieved in the limit of

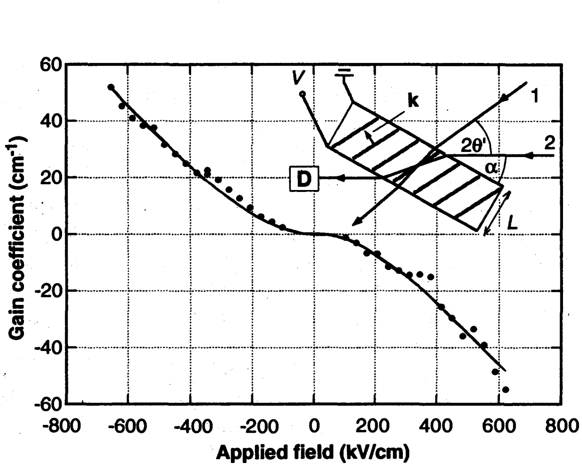

**Fig. 2.** The two-beam coupling gain coefficient of BisA-NAS:DEH 29% at large applied electric fields and 650-nm illumination wavelength. The solid line is a fit of the data to Eq. 2. The inset shows the geometry of the two-beam energy coupling measurements. D is a silicon photodiode detector, *V* is the applied voltage, **k** the grating wave vector, and *L* = 145 μm the sample thickness. The angle α between the probe beam 2 and sample surface was 30° and the angle 2θ between probe and pump beam 1 was 20°. The grating spacing Λ = 2.6 μm and the grating wave vector is oriented 63.6° from sample normal.

large $E_o$), and $E_d = k_B T\, k/e = 0.617$ kV/cm is the diffusion field. Here, $\epsilon_r = 3.5 \pm 0.3$ is the relative dielectric permittivity, $\epsilon_o$ is the vacuum permittivity, $e$ is the unit charge, $k_B$ is the Boltzmann constant, and $T = 297$ K is the temperature. The limiting space-charge electric field $E_q = 246 \pm 60$ kV/cm, determined by fitting the data of Fig. 2 to Eq. 2, is used to calculate the effective density of photorefractive charges $N_{PR} = 1.2 \pm 0.5 \times 10^{16}$ cm$^{-3}$ (*20*). Note that the calculated magnitude of the space-charge electric field $E_{sc} = 57$ kV/cm when $E_o = -655$ kV/cm in the low modulation ($m = 0.30$) measurements of Fig. 2 and $E_{sc} = 190$ kV/cm in the large modulation ($m = 1$) measurements mentioned earlier. The limiting space-charge electric field $E_q$ is significantly larger than has been achieved in inorganic photorefractive crystals, because of the much higher dielectric constants of the crystals (*13*).

The effective electrooptic response $n_0^3 r_{\text{eff}} = 6 \pm 1$ pm/V at a static applied electric field of 69 kV/cm was determined from the fit of the data in Fig. 2 to Eq. 2. The electrooptic coefficient of the same sample was measured directly with a Mach-Zehnder interferometer [taking electro-attraction and piezoelectric effects into account (*21*)] yielding a value of 0.7 ± 0.3 pm/V at 69 kV/cm. The apparent enhancement may be explained by a mechanism proposed recently (*22*), but further studies are necessary to confirm this.

The absorption coefficient exceeds the gain coefficient by a large margin over a wide range of wavelengths (Fig. 3). This means that the probe beam experiences net loss in traversing the sample. The gain coefficient decreases slowly with increasing wavelength (*23*), but the absorption coefficient of the polymer decreases exponentially with wavelength (the peak absorption of the dye molecule is at 408 nm) (Fig. 3). Therefore, extrapolation of the absorption and gain coefficient curves indicates that the gain at $E_o = -345$ kV/cm will exceed the absorption at ~740 nm and the gain at $E_o = -655$ kV/cm should exceed the absorption at ~710 nm. The probe beam should experience net gain at longer wavelengths which means that the probe beam gains intensity after passing through the sample. Net gain has been observed (at 753 nm) in another, lower gain, photorefractive polymer (*16*). Because many proposed applications of photorefractive polymers will use near infrared diode laser sources, the large absorption in the visible region is not a serious problem. Several samples of BisA-NAS:DEH 29% with and without buffer layers showed high dielectric strength (>250 kV/cm) and high gain coefficients (>5 cm$^{-1}$), demonstrating the repeatability of the sample fabrication process. A sample of BisA-NAT(nitroaminotolane):DEH 29% (*11*) had a gain coefficient curve similar to that of Fig. 2, but with maximum gain coefficient $g = 4.2$ cm$^{-1}$ at $E_o = -345$ kV/cm.

Assuming that the grating phase is 90°, the coupling strength should be $gL' \approx 2 \arcsin \sqrt{\eta}$, where $\eta$ is the holographic diffraction efficiency at modulation $m = 1$ (*24*). The diffraction efficiency $\eta = 12\%$ measured at an applied electric field of 345 kV/cm and wavelength of 650 nm in another sample of BisA-NAS:DEH 29% implies a gain coefficient of 44 cm$^{-1}$, in good agreement with the measured value of 33 cm$^{-1}$. The BisA-NAS:DEH photorefractive polymer has a response time of 0.11 s at 1 W/cm$^2$ at 650-nm wavelength (*14, 15*).

The present work demonstrates that the performance of photorefractive polymers can match or exceed that of the inorganic crystals. The improvement leading to the current results is the application of large electric fields to thick samples, facilitated by the use of buffer layers. Thicker samples have been made (*9*) and higher electric fields have been applied (*25*), but not both together because the breakdown voltage in thick samples occurs at defects and is only weakly dependent on thickness. The two-beam energy coupling gain coefficient increases approximately as the square of the applied electric field, which explains the dramatic increase in gain with modest increases in the applied electric field. The photorefractive model developed for crystals accurately describes the results reported here, without modifications tailored to organic systems such as have been proposed (*26*). High-performance photorefractive polymers may be incorporated into economical optical and opto-electronic devices in the near future because of their low cost and flexibility of fabrication. The two main hurdles to be overcome are the high absorption of the current polymers and the instability of the electrooptic coefficients.

**Fig. 3.** The absorption coefficient (triangles) and the two-beam energy coupling gain coefficient (circles) in BisA-NAS:DEH 29% at an applied electric field $E_o = -345$ kV/cm. The solid line through the gain coefficient data shows the expected dependence of gain on wavelength as discussed in the text. The single square datum is the gain at $E_o = -655$ kV/cm from Fig. 2.

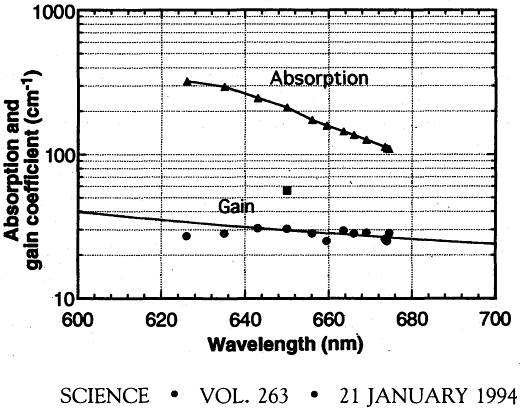

## REFERENCES AND NOTES

1. A. Ashkin *et al.*, *Appl. Phys. Lett.* **9**, 72 (1966).
2. J. O. White and A. Yariv, *ibid.* **37**, 5 (1980).
3. J. Feinberg and R. W. Hellwarth, *Opt. Lett.* **5**, 519 (1980).
4. D. Z. Anderson, D. M. Lininger, J. Feinberg, *ibid.* **12**, 123 (1987).
5. D. M. Lininger, *ibid.* **14**, 697 (1989).
6. D. Z. Anderson, *ibid.* **11**, 56 (1986).
7. J. Feinberg, *ibid.* **7**, 486 (1982).
8. J. Shamir, H. J. Caulfield, B. M. Hendrickson, *Appl. Opt.* **27**, 2912 (1988).
9. S. Ducharme, R. W. Twieg, J. C. Scott, W. E. Moerner, *Phys. Rev. Lett.* **66**, 1846 (1991).
10. C. A. Walsh and W. E. Moerner, *J. Opt. Soc. Am. B* **9**, 1642 (1992).
11. S. Ducharme, B. Jones, J. M. Takacs, L. Zhang, *Opt. Lett.* **18**, 152 (1993).
12. K. Tamura, A. B. Padias, J. H. K. Hall, N. Peyghambarian, *Appl. Phys. Lett.* **60**, 1803 (1992); X.-C. Zhang, X. F. Ma, Y. Jin, T.-M. Lu, *ibid.* **61**, 3080 (1992).
13. P. Günter and J.-P. Huignard, Eds., *Photorefractive Materials and Their Applications I: Fundamental Phenomena* (Springer-Verlag, Berlin, 1988), vol. 61, pp. 51–53.
14. B. Jones *et al.*, paper presented at the Annual Meeting of the Optical Society of America, Toronto, Canada, 3 to 8 October 1993; S. Ducharme *et al.*, *Proceedings of the Photorefractive Materials, Effects, and Devices Topical Meeting*, Kiev, Ukraine, 11 to 13 August 1993, B. Ya. Zeldovitch and E. Krätzig, Eds. (Ukrainian Academy of Sciences, Kiev, 1993), pp. 1–4.
15. B. E. Jones *et al.*, *J. Opt. Soc. Am. B*, in preparation; B. E. Jones, thesis, University of Nebraska (1993).
16. M. C. J. M. Donckers *et al.*, *Opt. Lett.* **18**, 1044 (1993).
17. A. S. Diamond, *Handbook of Imaging Materials* (Dekker, New York, 1991).
18. N. V. Kukhtarev, V. B. Markov, S. G. Odulov, M. S. Soskin, V. L. Vinetskii, *Ferroelectrics* **22**, 961 (1979).
19. We have assumed that the index of refraction is $n_o = 1.7$ and neglect birefringence.
20. P. Günter and J.-P. Huignard, Eds., in (*13*), pp. 82–84.
21. S. Ducharme and J. Feinberg, *IEEE J. Quantum Electron.* **23**, 2116 (1987).
22. W. E. Moerner, S. M. Silence, F. Hache, G. C. Bjorklund, *J. Opt. Soc. Am. B* **11**, in press.
23. Besides the explicit dependence of the gain coefficient on wavelength in Eqs. 2 and 3 (through $E_d$ and $E_q$), the electrooptic coefficient decreases with wavelength as a result of dispersion as described by Singer *et al.* [in *Nonlinear Optical Properties of Organic Molecules and Crystals*, D. S. Chemla and J. Zyss, Eds. (Academic Press, Orlando, FL, 1987), vol. 1, p. 449].
24. N. V. Kukhtarev, V. B. Markov, S. G. Odulov, M. S. Soskin, V. L. Vinetskii, *Ferroelectrics* **22**, 949 (1979).
25. T. Kawakami and N. Sonoda, *Appl. Phys. Lett.* **62**, 2167 (1993).
26. A. Twarowski, *J. Appl. Phys.* **65**, 2833 (1989); J. S. Schildkraut and A. V. Buettner, *ibid.* **72**, 1888 (1991).

27. Supported by a NSF Research Initiation Award (ECS-9209941) and by the Center for Materials Research and Analysis through the Nebraska Research Initiative.

4 August 1993; accepted 1 December 1993